BMB Reports - Manuscript Submission

Manuscript Draft

DOI: 10.5483/BMBRep.2022-0106

Manuscript Number: BMB-22-106

Title: α-Kleisin subunit of cohesin preserves the genome integrity of embryonic stem cells

Article Type: Article

Keywords: Cohesin; Embryonic stem cells; α-kleisin; Genomic integrity

Corresponding Author: Keun Pil Kim

Authors: Keun Pil Kim[1,*], Seobin Yoon[1], Eui-Hwan Choi[1], Eui-Hwan Choi[1,2], Eui-Hwan Choi[1,2], Seo Jung Park[1], Seo Jung Park[1]

Institution: [1]Department of Life Sciences, Chung-Ang University, [2]New Drug Development Center, Daegu-Gyeongbuk Medical Innovation Foundation,

BMB Reports

α-Kleisin subunit of cohesin preserves the genome integrity of embryonic stem cells

Seobin Yoon[1], Eui-Hwan Choi[1,2], Seo Jung Park[1], and Keun Pil Kim[1*]

[1]Department of Life Sciences, Chung-Ang University, Seoul 06974, Korea

[2]New Drug Development Center, Daegu-Gyeongbuk Medical Innovation Foundation, Daegu 41061, Korea

*To whom correspondence should be addressed.

Keun Pil Kim

Department of Life Sciences

Chung-Ang University

Seoul 06974

South Korea

E-mail: kpkim@cau.ac.kr

Phone: 82-2-820-5792

Fax: 82-2-820-5206

ABSTRACT

Cohesin is a ring-shaped protein complex that comprises the SMC1, SMC3, and α-kleisin proteins, STAG1/2/3 subunits, and auxiliary factors. Cohesin participates in chromatin remodeling, chromosome segregation, DNA replication, and gene expression regulation during the cell cycle. Mitosis-specific α-kleisin factor RAD21 and meiosis-specific α-kleisin factor REC8 are expressed in embryonic stem cells (ESCs) to maintain pluripotency. Here, we demonstrated that RAD21 and REC8 were involved in maintaining genomic stability and modulating chromatin modification in murine ESCs. When the kleisin subunits were depleted, DNA repair genes were downregulated, thereby reducing cell viability and causing replication protein A (RPA) accumulation. This finding suggested that the repair of exposed single-stranded DNA was inefficient. Furthermore, the depletion of kleisin subunits induced DNA hypermethylation by upregulating DNA methylation proteins. Thus, we proposed that the cohesin complex plays two distinct roles in chromatin remodeling and genomic integrity to ensure the maintenance of pluripotency in ESCs.

Keywords: cohesin; embryonic stem cells; α-kleisin; genomic integrity

INTRODUCTION

Embryonic stem cells (ESCs), which have unique properties such as pluripotency and unlimited self-renewal, exhibit unique expression patterns of genes related to chromosome topology, chromatin modification, and genomic integrity (1, 2). Cohesin is a ring-shaped protein complex composed of several subunits, structural maintenance of chromosome (SMC) family proteins, α-kleisin proteins, stromal antigen (STAG) proteins, and accessory factors (3-11). Furthermore, cohesin has two different combinations of subunits depending on the cell division stage: mitosis-specific subunits (RAD21) and meiosis-specific subunits (REC8 and RAD21L). During mitosis, the cohesin complex includes SMC1α, SMC3, RAD21, STAG1, and STAG2. Unlike the mitotic cohesin complex, SMC1β, which is the homolog of SMC1α, REC8, RAD21L, and STAG3, mainly functions in the chromosomes during meiosis (Fig. 1A) (12). The cohesin complex with REC8 appears on the chromosome during the prophase in meiosis I, and the complex remains until meiosis II, whereas the cohesin complex including RAD21L localizes along chromosome arms from the leptotene to the middle pachytene stage in prophase I and disappears after the late pachytene stage (12-14). RAD21 is also expressed during meiotic cell division (15, 16). The kleisin RAD21 is detected before early prophase I and disappears in early prophase I. Afterward, it reappears on chromosomes after the mid-late pachytene stage during the prophase stage of meiosis I (15, 16).

Our study revealed the role of the α-kleisin factors of the cohesin complex, REC8, and RAD21 in both chromatin modification and maintenance of genome integrity. Unlike in differentiated cells such as mouse embryonic fibroblast (MEF) cells, mitotic cohesin complex subunits and meiotic cohesin complex subunits are expressed in pluripotent states (17). Our findings demonstrated that the α-kleisin factors are constitutively expressed to function as safeguards of genome integrity throughout the entire cell cycle in ESCs and that the involvement of REC8 and RAD21 is important to modulate chromatin remodeling in the ESC cycle.

RESULTS

The α-kleisin subunits RAD21 and REC8 are abundantly expressed in mouse ESCs throughout the cell cycle

To explore the expression dynamics of α-kleisin factors during the cell cycle, we synchronized ESCs and MEFs at the G1/S phase via the double thymidine block and released them from the G1/S phase (Fig. 1B). Our findings indicated that the α-kleisin factors REC8 and RAD21 were constitutively expressed regardless of the cell cycle phase of the ESCs (Fig. 1C). However, in contrast to ESCs, MEFs expressed RAD21, not REC8, during cell cycle progression. Particularly, cohesin builds cohesion during DNA replication because sister chromatids are generated by replication during the S phase (18). Therefore, we further focused on the expression levels of cohesin factors during the S phase (i.e., 2.5 h after the cell cycle arrest is released by the double thymidine block). The expression of RAD21 in ESCs

at the protein and RNA levels exhibited 1.71- and 4.57-fold differences relative to MEFs, respectively (Fig. 1D). Additionally, REC8 was expressed at the protein and RNA levels in ESCs but not in MEFs (Fig. 1D-F) (17). Furthermore, the RNA expression levels of the factors in ESCs were different from those in MEFs. RNA sequencing and real-time PCR (RT-PCR) analyses revealed that the α-kleisin factors were expressed in ESCs but not in MEFs (Fig. 1E, F). Additionally, the RNA expression levels of diverse factors involved in meiotic or mitotic cohesin subunits in ESCs were higher than those in MEFs (Fig. 1E, F).

In the Kyoto Encyclopedia of Genes and Genomes (KEGG) analysis, we demonstrated that REC8 or RAD21 depletion could differentially regulate numerous genes in ESCs (Supplementary Fig. 1 and 2). Therefore, we classified KEGG pathways according to the number of genes whose expression levels were differentially regulated by REC8 or RAD21 depletion. Furthermore, the depletion of each cohesin factor enables the differentiation of ESCs into specific cell-type lineages (19).

Depletion of cohesin decreases DNA repair efficiency

In ESCs, homologous recombination (HR) is a major DNA repair system, and the factors involved in the HR-mediated repair system are highly expressed compared with those in MEFs, which result from the prolonged S phase and rapid cell cycle progression (17, 20, 21). Furthermore, we found that the replication protein A (RPA) focal number in ESCs was higher than that in MEFs, and the cohesin intensity of ESCs was higher than that of MEFs (Fig. 2A, B). When cohesin factors were depleted, there was an increase in the number of RPA foci, which bind to single-stranded DNA to prevent the strand from forming a secondary structure (Fig. 2C, D, I, Supplementary Fig. 3A-C). We observed that the expression of each factor decreased under the depleted condition. Particularly, REC8 and RAD21 expression decreased by 55%–70% and 70%–80%, respectively (Fig. 2C, D, G, H, Supplementary Fig. 3A, B, D, E). Furthermore, the average number of RPA foci in REC8-depleted ESCs was approximately 27.26, whereas the average number of RPA foci in RAD21-depleted ESCs was approximately 36. The RPA focal number under the REC8 depletion condition was 1.7~2 times that of the control (Fig. 2C, G, Supplementary Fig. 3A, C). Accordingly, the number of RPA foci increased dramatically in the RAD21-depleted ESCs by as much as 2.33–2.8-fold compared with that of the control (Fig. 2D, I, Supplementary Fig. 3B, C). Likewise, siRAD21-treated MEF cells exhibited higher RPA focal numbers than the siControl cells. The RPA focal number was significantly increased to 37 in RAD21-depleted cells (Fig. 2E, F, J). Conversely, the RPA focal number in REC8-depleted cells was 1.2, which was similar to the siControl cells (RPA foci in siControl cell = 1.36).

To confirm the role of the cohesin complex in DNA damage repair and replication stress, we depleted either RAD21 or REC8 in ESCs treated with hydroxyurea (HU). This impedes DNA replication by inhibiting ribonucleotide reductase (RNR), which converts ribonucleotides into deoxyribonucleotides (Fig. 2K) (22). Cohesion occurs in DNA replication to hold sister chromatids (17,

18, 23-26). Thus, we used HU to induce the stalling of DNA replication and impede cell cycle progression to arrest at the S phase. The expression of the kleisin subunits decreased, which resulted from the depletion of the factors after treating the cells with siRNA against REC8 or RAD21 (Supplementary Fig. 3F). In ESCs, RPA focus formation significantly increased upon REC8 depletion with HU and RAD21 depletion with HU (Fig. 2L-N). When the cells were treated with HU only, the RPA focal number was approximately 66.97. Conversely, RPA focal formation increased when both kleisin subunits were depleted (approximately 80.5 foci in REC8-depleted cells and 92.9 foci in RAD21-depleted cells).

Depletion of cohesin decreases cell viability by reducing HR-mediated DNA repair efficiency

To confirm cell viability under cohesin depletion and ectopic expression, cell viability was analyzed with thiazole orange (TO) and propidium iodide (PI) staining. Three siRNA candidates against REC8 or RAD21 were applied to validate their depletion efficiency through protein analysis and cell viability test (Supplementary Fig. 4, siREC8 #1 and siRAD21 #1 were used in this study). We then transfected the cells with pDR-GFP and pCBA-SceI to confirm the efficiency of homologous recombination (HR), which is considered an error-free DNA repair system. The HR efficiency of the siControl cells was 10.1%, whereas those of the REC8- and RAD21-depleted stem cells were 4.42% and 4.28%, respectively (Supplementary Fig. 5A). Furthermore, cell viability was not affected by the depletion or ectopic expression of REC8 in MEFs (Supplementary Fig. 5B-E). Live cells accounted for 91.9% of all cells under the control condition, whereas viability decreased in the REC8- or RAD21-depleted ESCs (Fig. 3A-D). Specifically, when the REC8 level decreased, the live ESC population decreased to approximately 84% of the total cells; when RAD21 was depleted, the normal cell population was 74.4%. Additionally, the live population of HU-treated cells was approximately 67.5% (Fig. 3A-D). However, the ectopic expression of RAD21 or REC8 did not significantly affect cell viability compared with that of depletion because the expression levels of other cohesin subunits likely did not change. We further analyzed RNA sequencing data from REC8- and RAD21-depleted ESCs to confirm the expression levels of DNA repair genes. In REC8-depleted ESCs, 48 genes related to DNA repair were upregulated, whereas 116 were downregulated. In RAD21-depleted ESCs, 73 genes were upregulated, and 154 genes were downregulated. REC8 and RAD21-depleted cells shared 20 upregulated genes and 76 downregulated genes (Fig. 3E, F). Next, the significantly downregulated genes under both conditions were assigned to different functional classifications. The top 10 classifications were then ranked according to the number of downregulated genes. Genes associated with DNA repair, DNA damage stimulus, double-strand break repair, DNA replication, and DNA replication were downregulated in REC8- and RAD21-depleted ESCs (Fig. 3G). Interestingly, many genes involved in DNA repair interacted with RAD21 and REC8. Among the genes that interacted with these α-kleisin factors, DNA repair genes bound more strongly (Supplementary Fig. 6).

The cohesin complex is involved in DNA methylation

In embryonic stem cells, DNA methylation plays an essential role in cell development and differentiation (27, 28). Patients with cohesinopathies (i.e., diseases caused by mutations in the cohesin complex) such as CdLS (Cornelia de Lange Syndrome) and Roberts syndrome exhibit abnormal DNA methylation patterns, resulting in changes in transcriptional regulation (29). Therefore, we investigated the effects of cohesin depletion on the dynamics of DNA methylation. Cells treated with siRNA against cohesin were stained with anti-5-methylated cytosine (5mC) antibodies to investigate the relationship between cohesin and DNA methylation in ESCs. DNA methyltransferases, namely, DNMT1, DNMT3a, and DNMT3b, play an important role in ESC differentiation and cell fate (30-33). The expression level of DNMT3b, the main *de novo* DNA methyltransferase, was increased in REC8- or RAD21-depleted ESCs (Fig. 4A, B). The average fluorescence intensity of 5mC in the control ESCs was approximately 41.4 ± 18. Under REC8 or RAD21 depletion, the DNA methylation level increased compared with that of the control. The average intensity in REC8-depleted ESCs was approximately 78.2 ± 10.3, whereas the average intensity in RAD21-depleted ESCs was approximately 90.9 ± 19.3 (Fig. 4C, D).

Differentiation was induced with RA in ESCs, and the DNA methylation level was analyzed by staining the cells with anti-5mC antibodies. The intensity of the 5mC signal increased as early as 24 h after the cells were treated with RA. As the ESCs lost their pluripotency, the fluorescence intensity of 5mC gradually decreased accordingly (Supplementary Fig. 7). However, 96 h after the RA treatment, the DNA methylation level was similar to that of differentiated cells (MEFs), suggesting that the DNA methylation pattern could be changed dynamically during ESC differentiation.

DISCUSSION

Unlike the differentiated cells, ESCs have a unique gene expression landscape that can be attributed to the cell cycle pattern (i.e., prolonged S phase), pluripotency, and self-renewal abilities (17, 20, 21). Interestingly, ESCs express REC8 and RAD21, which are involved in chromosome segregation, cohesion, and topology (17). Our study provided novel insights into the involvement of the α-kleisin factors RAD21 and REC8 in the maintenance of genomic integrity and chromatin methylation to manage the self-renewal of ESCs and enhance the efficiency of ESC differentiation.

Our findings demonstrated that REC8 and RAD21 were expressed in ESCs regardless of the cell cycle phase (Fig. 1C). Furthermore, ESCs constitutively express HR proteins and facilitate HR-mediated DNA repair during the cell cycle. Therefore, under the DNA damage condition, RPA foci formation increased, and the expression of the kleisin factors increased significantly (Fig. 2C–N), suggesting that these two factors are closely related to DNA damage repair. Therefore, the depletion of cohesin interfered with HR-mediated DNA repair, and the proportion of apoptotic cells increased in kleisin-depleted ESCs. Cohesin depletion in ESCs led to the downregulation of diverse genes involved

in DNA repair, DNA damage responses, and genomic integrity compared with ESCs with the normal cohesin complex (Fig. 3E-G). Moreover, α-kleisin was strongly correlated with the interaction with DNA repair genes (Supplementary Fig. 6). Our results suggested that cohesin could support the maintenance of genome integrity (Fig 4E).

We further demonstrated that the DNA methylation level was lower in differentiated cells than in undifferentiated ESCs. Furthermore, the abnormal establishment of the cohesin complex resulting from REC8 or RAD21 depletion causes hypermethylation by increasing the expression level of the *de novo* methyltransferase DNMT3b (Fig. 4A-E). During cell differentiation, the DNA methylation pattern was dynamically changed to control gene expression by regulating gene expression to restrict the lineage (29, 30). Thus, we propose that the depletion of cohesin factors led to DNA hypermethylation, which presumably changed gene expression and chromosome structure.

MATERIALS AND METHODS

Materials and methods are available in the supplemental material.

ACKNOWLEDGMENTS

We thank Soojin Lee of Chung-Ang University for helping in the preparation of the REC8 plasmid. This work was supported by grants to K.P.K. from the National Research Foundation of Korea, funded by the Ministry of Science, ICT, & Future Planning (No. 2020R1A2C2011887; 2018R1A5A1025077).

CONFLICTS OF INTEREST

The authors declare no conflict of interest.

REFERENCES

1. Young RA (2011) Control of the embryonic stem cell state. Cell 144, 940–954.

2. Bhattacharya B, Miura T, Brandenberger R. et al. (2004) Gene expression in human embryonic stem cell lines: Unique molecular signature. Blood 100, 2956–2964.

3. Deb S, Xu H, Tuynman J et al. (2014) RAD21 cohesin overexpression is a prognostic and predictive marker exacerbating poor prognosis in KRAS mutant colorectal carcinomas. Br. J. Cancer 110, 1606–1613.

4. Birkenbihl RP and Subramani S (1992) Cloning and characterization of rad21 an essential gene of *Schizosaccharomyces pombe* involved in DNA double-strand-break repair. Nucleic Acids Res 20, 6605–6611.

5. Nasmyth K, Peters JM and Uhlmann F (2001) Splitting the chromosome: Cutting the ties that bind sister chromatids. Science 288. 113–138.

6. Sonoda E, Matsusaka T, Morrison C et al. (2001) Scc1/Rad21/Mcd1 is required for sister chromatid

cohesion and kinetochore function in vertebrate cells. Dev Cell 1, 759–770.

7. Bauerschmidt C, Arrichiello C, Burdak-Rothkamm S et al. (2009) Cohesin promotes the repair of ionizing radiation-induced DNA double-strand breaks in replicated chromatin. Nucleic Acids Res 38, 477–487.

8. Xu H, Balakrishnan K, Malaterre J et al. (2010) Rad21-cohesin haploinsufficiency impedes DNA repair and enhances gastrointestinal radiosensitivity in mice. PLoS One 5, e12112.

9. Watrin E and Peters JM (2009) The cohesin complex is required for the DNA damage-induced G2/M checkpoint in mammalian cells. EMBO J 28, 2625–2635.

10. Supernat A, Łapińska-Szumczyk S, Sawicki S, Wydra D, Biernat W and Żaczek AJ (2012) Deregulation of RAD21 and RUNX1 expression in endometrial cancer. Oncol Lett 4, 727–732.

11. Hakimi MA, Bochar DA, Schmiesing JA et al. (2002) A chromatin remodelling complex that loads cohesin onto human chromosomes. Nature 418, 994–998.

12. Ishiguro K. (2019) The cohesin complex in mammalian meiosis. Genes to Cells 24, 6–30.

13. Ishiguro K, Kim J, Shibuya H et al. (2014) Meiosis-specific cohesin mediates homolog recognition in mouse spermatocytes. Genes Dev 28, 594–607.

14. Lee J and Hirano T (2011) RAD21L, a novel cohesin subunit implicated in linking homologous chromosomes in mammalian meiosis. J Cell Biol 192, 263–276.

15. Eijpe M, Offenberg H, Jessberger R, Revenkova E and Heyting C (2003) Meiotic cohesin REC8 marks the axial elements of rat synaptonemal complexes before cohesins SMC1β and SMC3. J Cell Biol 160, 657–670.

16. Biswas U, Hempel K, Llano E, Pendas A and Jessberger R (2016) Distinct roles of meiosis-specific cohesin complexes in mammalian spermatogenesis. PLoS Genet 12, e1006389.

17. Choi EH, Yoon S, Koh YE et al. (2022) Meiosis-specific cohesin complexes display essential and distinct roles in mitotic embryonic stem cell chromosomes. Genome Biol. 23, 70

18. Uhlmann F and Nasmyth K (1998) Cohesion between sister chromatids must be established during DNA replication. Curr Biol 8, 1095–1101.

19. Koh YE, Choi E, Kim J, and Kim KP (2022) The kleisin subunits of cohesin are involved in the fate determination of embryonic stem cells. Mols Cells 45, 820-832.

20. Yoon SW, Kim DK, Kim KP and Park KS (2014) Rad51 regulates cell cycle progression by preserving G2/M transition in mouse embryonic stem cells. Curr Biol 23, 2700–2711.

21. Choi EH, Yoon S, Park KS and Kim KP (2017) The homologous recombination machinery orchestrates post-replication DNA repair during self-renewal of mouse embryonic stem cells. Sci Rep 7, 11610.

22. Aye Y, Li M, Long MJC and Weiss RS (2015) Ribonucleotide reductase and cancer: Biological mechanisms and targeted therapies. Oncogene 34, 2011–2021.

23. Choi EH, Yoon S, Koh YE, Seo YJ and Kim KP (2020) Maintenance of genome integrity and active

homologous recombination in embryonic stem cells. Exp Mol Med 52, 1220–1229.

24. Nasmyth K and Hearing CH (2009) Cohesin: its roles and mechanisms. Annu Rev Genet 43, 525–558.

25. Peters JM, Tedeschi A and Schmitz J (2008) The cohesin complex and its roles in chromosome biology. Genes Dev 22, 3089–3114.

26. Onn I, Heidinger-Pauli JM, Guacci V, Unal E and Koshland DE (2008) Sister chromatid cohesion: a simple concept with a complex reality. Annu Rev Cell Dev Biol 24, 105–129.

27. Okano M, Bell DW, Haber DA and Li E (1999) DNA methyltransferases Dnmt3a and Dnmt3b are essential for de novo methylation and mammalian development. Cell 99, 247-257.

28. Li E, Bestor TH and Jaenisch R (1992) Targeted mutation of the DNA methyltransferase gene results in embryonic lethality. Cell 69, 915-926.

29. Liu J, Zhang Z, Bando M et al. (2010) Genome-wide DNA methylation analysis in cohesin mutant human cell lines. Nucleic Acids Res 38, 5657-5671.

30. Geiman TM, Sankpal UT, Robertson AK et al. (2004) Isolation and characterization of a novel DNA methyltransferase complex linking DNMT3B with components of the mitotic chromosome condensation machinery. Nucleic Acids Res 32, 2716–2729.

31. Jeziorska DM, Murray RJS, De Gobbi M et al. (2017) DNA methylation of intragenic CpG islands depends on their transcriptional activity during differentiation and disease. Proc Natl Acad Sci 114, E7526–7535.

32. Leppert S and Matarazzo MR (2014) De novo DNMTs and DNA methylation: novel insights into disease pathogenesis and therapy from epigenomics. Curr Pharm Des 20, 1812–1818.

33. Lurlaro M, Von Meyenn F and Reik W (2017) DNA methylation homeostasis in human and mouse development. Curr Opin Genet Dev 43, 101–109.

FIGURE LEGENDS

Fig. 1. Expression levels of cohesin complex factors in ESCs. (A) Mitotic and meiotic cohesin complex model. The mitotic cohesin complex includes SMC1α, RAD21, and STAG1/2. The meiotic cohesin complex contains SMC1β and REC8 instead of the mitotic cohesin components. (B) Scheme of the time course of the experiments. ESCs were synchronized by double thymidine and were released for cell cycle progression. (C) Expression levels of cohesin components in ESCs. After a double thymidine block, the cells were released for cell cycle progression as shown in (B). (D) Expression levels of α-kleisin factors during the S phase. The expression levels of cohesin REC8 and RAD21 were compared during the S phase through western blot analysis and RNA sequencing analysis. (E, F) RNA analysis for cohesin-related genes in undifferentiated and differentiated cells. The transcript levels of the genes involved in cohesin function were analyzed by RNA sequencing (E) and qPCR (F). The primers used in the qPCR analysis were described by Choi et al. (17). The transcript levels were

determined by taking the average of two independent analyses from RNA sequencing. After obtaining the qPCR data, the relative expression of the target genes was calculated by using the housekeeping gene 18s rRNA. Three independent experiments were performed, and the error bars represent the mean ± SD.

Fig. 2. Involvement of the cohesin complex in HR-mediated DNA repair mechanism. (A–D) α-Kleisin factor and RPA staining in ESCs and MEFs. ESCs and MEFs were immunostained against RPA and REC8 (A, C) and against RPA and RAD21 (B, D). ESCs and MEFs were untreated (normal condition) (A, B) and REC8 or RAD21 were depleted in ESCs (C, D). (E, F) RPA focal formation in REC8- or RAD21-depleted MEFs. (G, H) Quantification of cohesin intensity. ESCs were treated with siRNA against REC8 or RAD21, after which the intensity of each kleisin factor was measured. The error bars indicate mean ± standard deviations (SD; N = 40 for each experiment). The number of RPA foci was quantified in kleisin-depleted ESCs (I) or MEFs (J) treated with siREC8 or siRAD21 (N = 120, three independent experiments for ESCs; N = 80, two independent experiments for MEF). (K) Schematic of the treatment of cells with siRNA against REC8 or RAD21 and hydroxyurea (HU). (L, M) Increase in the intensity of REC8 or RAD21 and RPA focal formation in DNA-damaged and DNA-depleted ESCs. (N) Measurement of RPA focal number. The blue, green, and orange bars indicate the average of each experiment (N = 3). The values represent the RPA foci per nucleus of 40 cells per experiment.

Fig. 3. Involvement of α-kleisin factor in the maintenance of genome integrity of ESCs. (A) Decrease in cell viability under REC8 or RAD21 depletion and DNA damage. (B) Cell viability analysis in cohesin-expressed ESCs with or without DNA damage by using HU. The apoptotic cells and live cells were analyzed by cell staining with PI and TO. (C, D) Quantification of the proportion of live cells and apoptotic cells. The cell survival rate was determined by flow cytometry and quantified with the BD Accuri C6 software. (E) Venn diagram illustrating the upregulated and downregulated genes when REC8 or RAD21 was depleted in ESCs. The red and blue numbers indicate the upregulated and downregulated genes in REC8- or RAD21-depleted ESCs relative to the siControl-treated ESCs. The black numbers represent the genes with the same RNA expression level in REC8- and RAD21-depleted ESCs and siControl-treated ESCs. The data were adjusted with $p \leq 0.05$. (F) Heatmap of the expression of DNA repair genes relative to the siControl group. Red indicates upregulation, blue indicates downregulation, and white indicates the same expression. (G) Gene set enrichment analysis (GSEA) score of REC8- or RAD21-depleted ESCs for downregulated DNA repair genes. GSEA was performed through two independent experiments.

Fig. 4. Cohesin depletion induces DNA hypermethylation. (A) DNA methyltransferase expression

level in REC8- or RAD21-depleted ESCs via immunoblot analysis. The expression level of DNMT3b was measured in kleisin factor-depleted undifferentiated cells compared with that in the control cells (B). (C) Representative images of DNA methylation in REC8- or RAD21-depleted ESCs. 5mC was used to stain the siControl-, siREC8-, and siRAD21-treated ESCs. (D) Increase in 5mC-staining intensity due to the presence of the abnormal cohesin complex in ESCs. (E) Model of α-kleisin factor functions. Depletion of the α-kleisin factors REC8 or RAD21 in the cohesin complex promoted DNA hypermethylation and accumulation of DNA gaps.

Figure 1

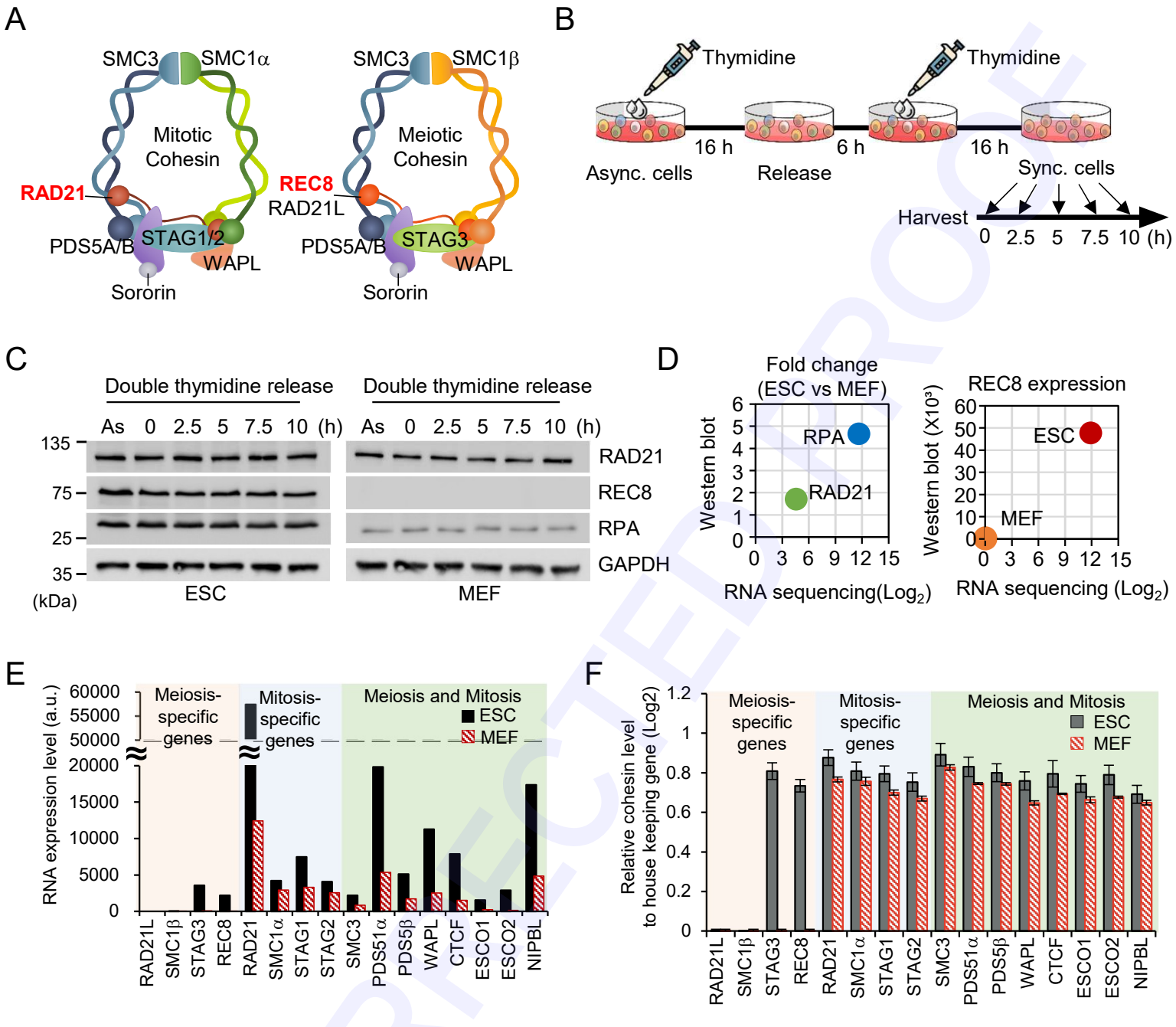

Figure 2

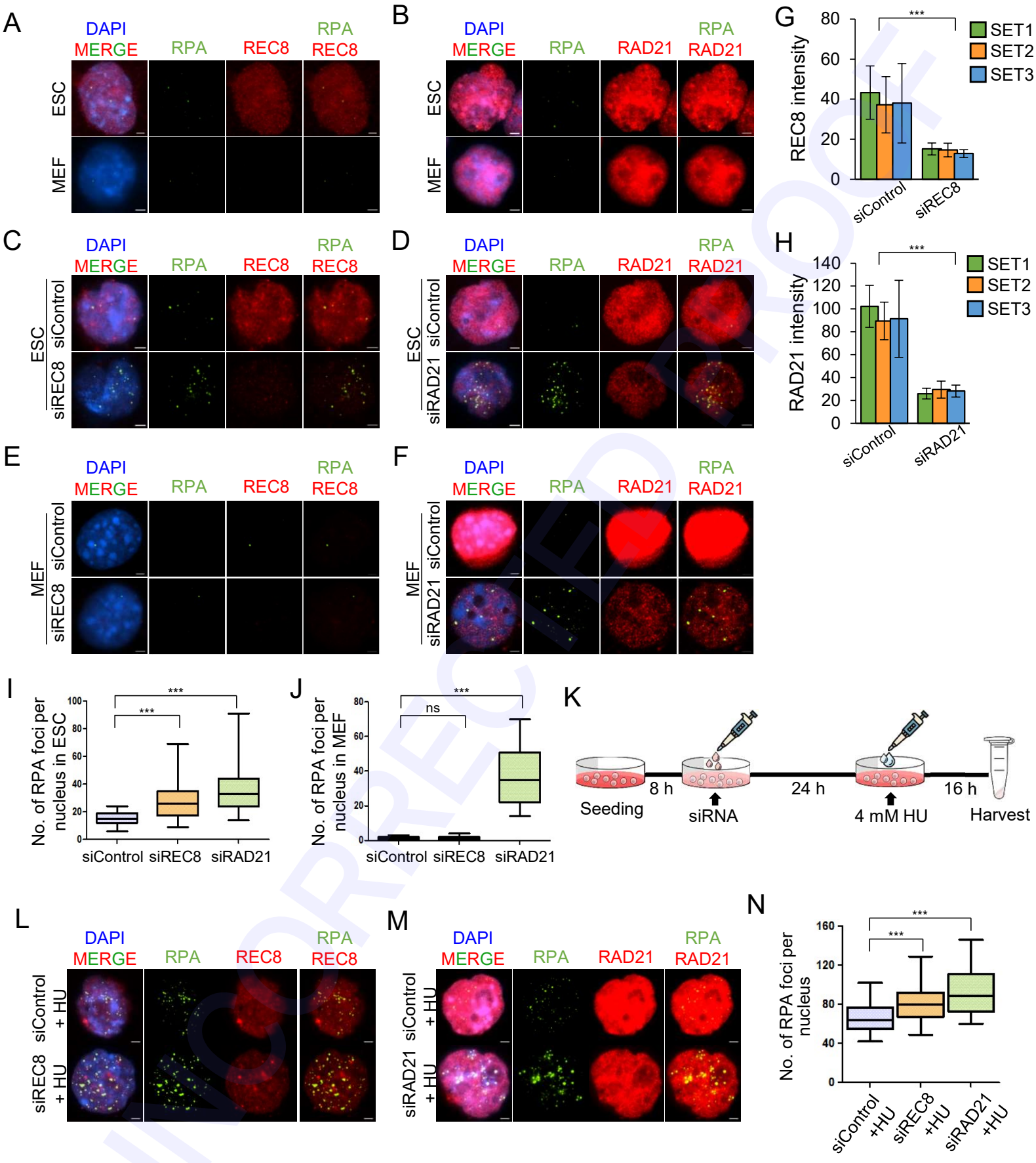

Figure 3

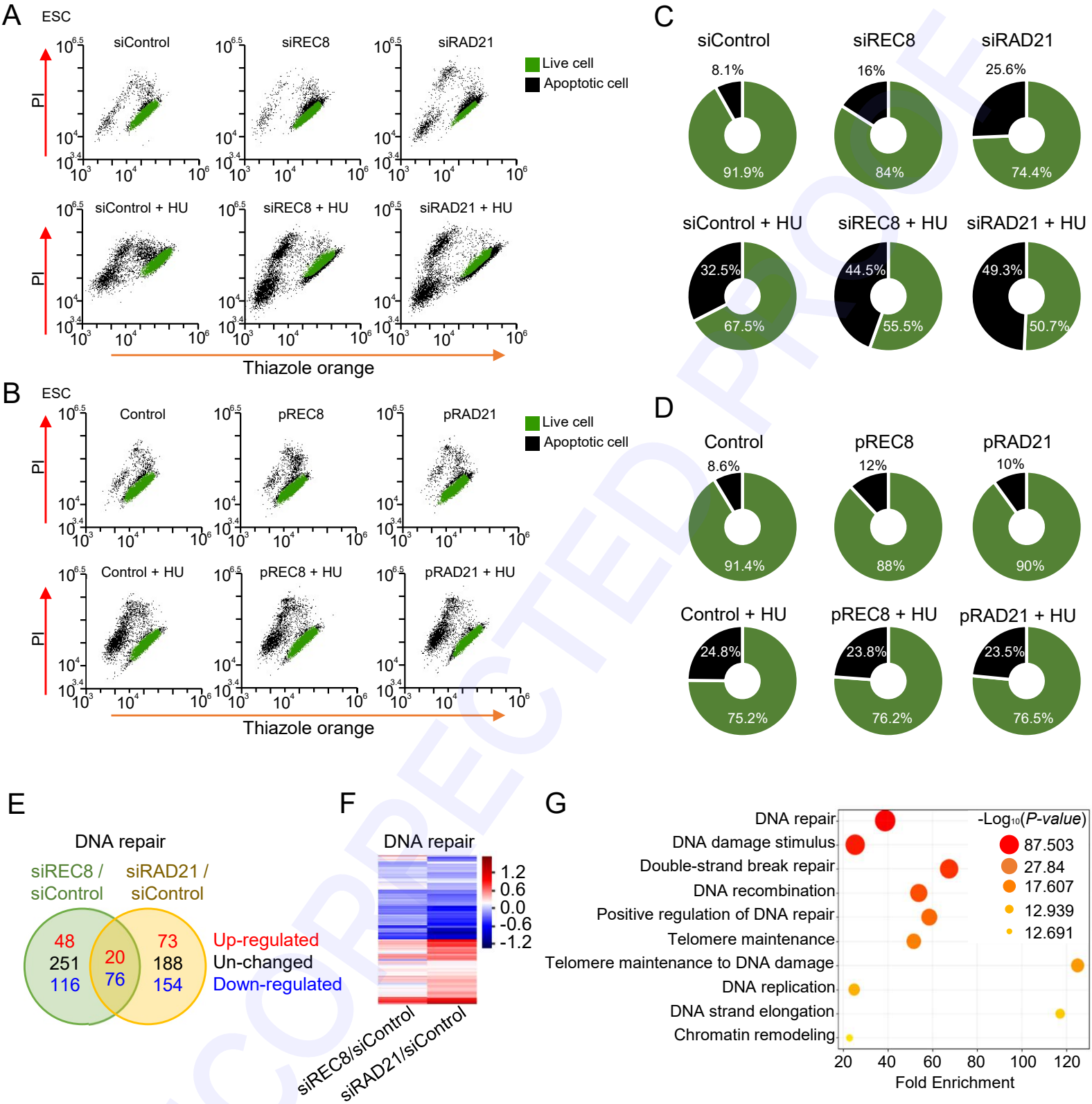

Figure 4

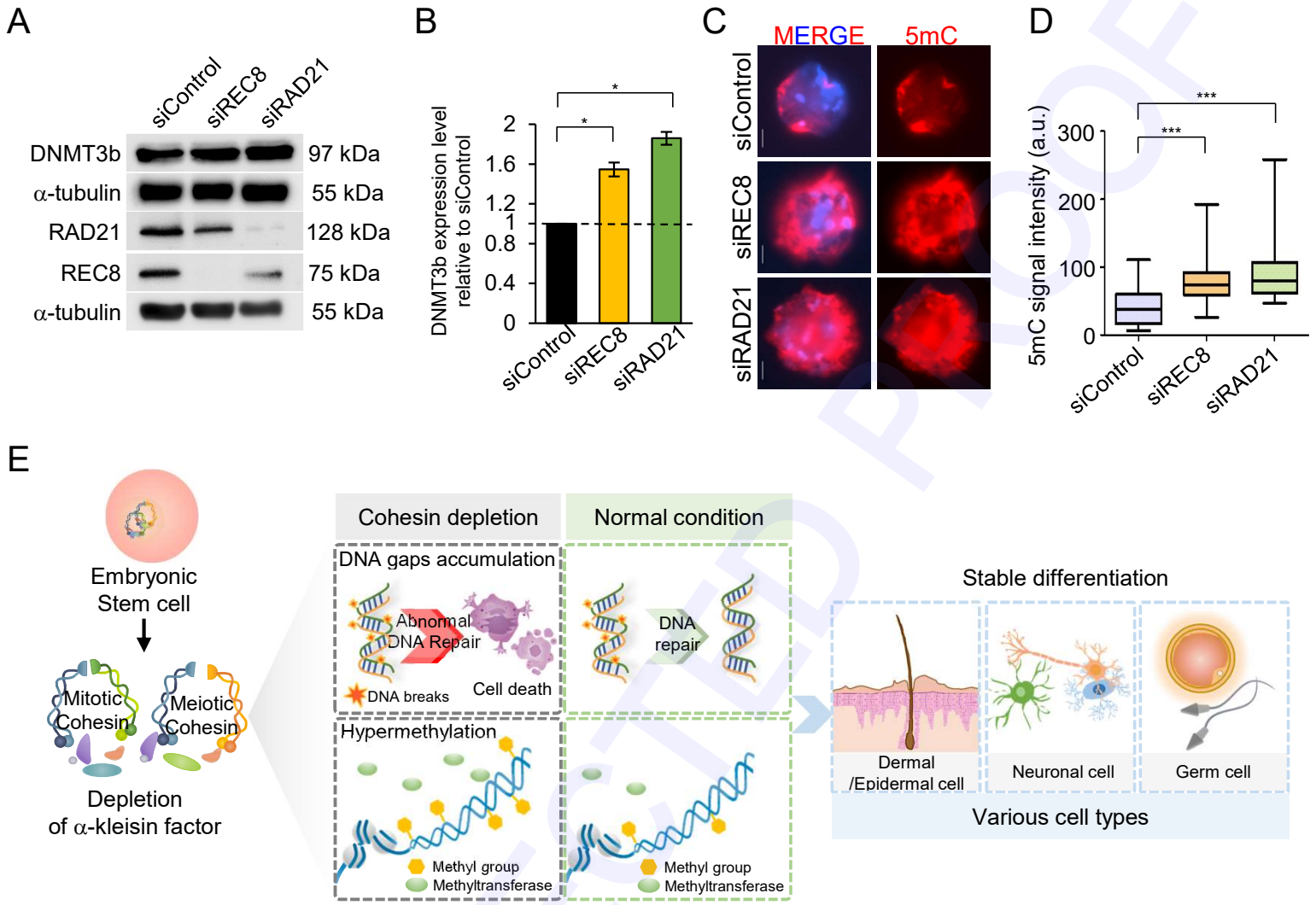

Supplementary Information

α-Kleisin subunit of cohesin preserves the genome integrity of embryonic stem cells

Seobin Yoon[1], Eui-Hwan Choi[1,2], Seo Jung Park[1], and Keun Pil Kim[1*]

[1]Department of Life Sciences, Chung-Ang University, Seoul 06974, Korea

[2]New Drug Development Center, Daegu-Gyeongbuk Medical Innovation Foundation, Daegu 41061, Korea

Supplementary Methods

Cell culture

J1 murine ESCs and MEFs were cultured as described previously (17, 18). J1 cells were cultured in DMEM plus GlutaMAX-I (GIBCO, Waltham, MA, USA) supplemented with 10% (v/v) horse serum (GIBCO), 2 mM L-glutamine (GIBCO), 0.1 mM Minimum Essential Medium Non-Essential Amino Acids (GIBCO), 100 U/ml penicillin-100 mg/ml streptomycin (GIBCO), 10 mM HEPES (GIBCO), 0.1 mM β-mercaptoethanol (GIBCO), and 1,000 U/ml mouse ESGRO leukemia inhibitory factor (LIF; Millipore, Billerica, MA, USA). MEFs were cultured in DMEM, which was supplemented with 100 U/ml penicillin-100 μg/ml streptomycin (GIBCO) and 10% (v/v) fetal bovine serum (GIBCO). The cells were incubated at 37 °C in a humified incubator with 5% CO_2.

RNA interference

Small interfering RNAs (siRNAs) against RAD21, REC8, and control were prepared from Bioneer (Daejeon, South Korea). The siRNA sequences are shown in Supplementary Table 1. The oligonucleotides were used to deplete each endogenous cohesin complex subunit (REC8 and RAD21) by using Lipofectamine (Invitrogen, Carlsbad, CA, USA). The cells were treated with siRNA in opti-MEM plus GlutaMAX medium and incubated in a humified incubator at 37 °C with 5% CO_2 for 48 h.

Cell synchronization

G1-S synchronized cells, J1 or MEF, were prepared as described previously (19). The cells were synchronized at the G1–S checkpoint with 2 mM thymidine for 16 h. After thymidine treatment, the cells were washed with phosphate-buffered saline (PBS) and released by replacing the fresh media for 6 h. Then, 2 mM thymidine was added to the cells for double thymidine synchronization, and the cells were incubated for 16 h. After double thymidine synchronization, the cells were harvested at 0, 2.5, 5, 7.5 and 10 h after the thymidine block was released.

5mC detection

Cell samples were harvested and attached to poly-L-lysine-coated coverslips. The cells were fixed with 4% paraformaldehyde and permeabilized with 0.2% Triton X-100. The samples were denatured with 4 N HCl and then neutralized with 100 mM Tris-HCl (pH 8.5). The cells were blocked with 1% bovine serum albumin (BSA) in phosphate-buffered saline with 0.1% Tween 20 (PBST) and then incubated with anti-5-methylcytosine antibody (EpiGentek, Farmingdale, NY, USA) for 1 h. After incubation, the samples were washed with PBST thrice and incubated with secondary antibodies conjugated with tetramethylrhodamine (TRITC; Jackson ImmunoResearch). The stained cells were washed with PBST and completely dried. After being dried, the samples were covered with an antifade mounting solution (Thermo Scientific, Rockford, IL, USA). Images were taken using an Eclipse Ti-E fluorescence

microscope (Nikon Eclipse, Tokyo, Japan).

FACS analysis for homologous recombination efficiency

ESCs were transfected using the pDR-GFP plasmid. The cells were treated with puromycin to select the cells with the plasmid. The clones containing the pDR-GFP plasmid were transfected with pCBASceI to digest the recognition site and induce the repair system. A green fluorescent protein (GFP) signal was produced through inducible homologous recombination. The samples were then analyzed with a FACSCalibur flow cytometer.

Induction of cell differentiation

ESC differentiation was induced by adding 0.2 μM of all-*trans*-RA (R2625, Sigma) to the culture media without LIF for 24, 48, 72, and 96 h.

RNA isolation

Total mRNA was isolated using an RNeasy mini kit (Qiagen) in accordance with the manufacturer's instructions. RNA was quantified with Multiskan GO (ND-2000, Thermo Fisher).

RNA library generation and sequencing

A library of RNA and RNA sequencing was generated in accordance with the methods described by Choi *et al*. (17). Total RNA was extracted from the cells by using the RNeasy mini kit (Qiagen), and cDNA was synthesized with a cDNA synthesis kit in accordance with the manufacturer's instruction (Enzynomics, Daejeon, Korea). Indexing was performed with illumine indices 1–12 (Illumina, San Diego, CA, USA). The enrichment step was conducted via polymerase chain reaction. Then, the average of the fragment size of the libraries was checked using an Agilent 2100 bioanalyzer (DNA high-sensitivity kit). Quantification was performed using the library quantification kit with a StepOne Real-Time PCR System (Life Technologies, Waltham, MA USA). High-throughput paired-end 100 sequencing was performed using a HiSeq X10 sequencer. Data were analyzed with ExDEGA software (E-biogen, Seoul, Korea).

REC8 overexpression

The cDNA of the gene was subcloned into a manipulated pcDNA6/myc-His A vector modified with an EF-1α promoter and 6-hemagglutinin (HA) tag (KpnI/EcoRI sites for REC8) to induce REC8 overexpression. Then, 2 μg of DNA was mixed with polyethylenimine (PEI) and added to the cultured cells to transfect the cloned plasmid DNA. The transfected cells were harvested at 24, 48, 72, and 98 h after the DNA–PEI mixture was added.

Cell viability analysis

The samples under each condition were harvested and stained with TO (BD, 349483) and PI (BD, 349483). The stained cells were incubated at 25 °C for 5 min. Cell viability was measured via FACS analysis by using a FACSCalibur flow cytometer.

Immunofluorescence analysis

Cells were stained as described previously (17). Primary antibodies against RAD21 (Abcam), REC8 (this antibody recognized a REC8 recombinant C-terminal 342 amino acid sequence) (17), and RPA (Millipore) were used. The following secondary antibodies were used: TRITC (Jackson ImmunoResearch) and fluorescein isothiocyanate (Jackson ImmunoResearch). Images were captured using an Eclipse Ti-E fluorescence microscope (Nikon Eclipse).

Western blot analysis

The samples were prepared as described previously (17). The following primary antibodies were used: RAD21 (Abcam, Cambridge, MA, USA), Rec8 (Abcam), RPA (Cell Signaling Biotechnology, Danvers, MA, USA), GAPDH (Abcam), OCT4 (Santa Cruz, CA, USA), DNMT3b (abcam), and α-tubulin (Abcam). The following secondary antibodies were used: Peroxidase AffiniPure goat anti-mouse IgG (Jackson ImmunoResearch, West Grove, PA, USA) and Peroxidase AffiniPure goat anti-rabbit IgG (Jackson ImmunoResearch). Immunoactivity was determined using an ECL solution.

KEGG analysis

KEGG (Kyoto Encyclopedia of Genes and Genomes) was performed by RNA sequencing with REC8-knocked down ESCs or RAD21-knocked down ESCs. Genes that were regulated by REC8 depletion or RAD21 depletion were selected and sorted into upregulated or downregulated genes. KEGG analysis was performed under the following conditions: normalized data (log2) > 4, $p < 0.05$ and fold-change relative to siControl < 0.8 in downregulated genes or fold-change relative to siControl > 1.25 in upregulated genes. The genes were classified according to the related pathway by using the KEGG mapper (https://www.genome.jp/kegg/).

Statistical analysis

Data were statistically analyzed using GraphPad Prism 5. Statistically significant differences between the comparison and control groups were determined with a paired two-tailed t-test (*$p < 0.05$, **$p < 0.01$, and ***$p < 0.001$).

Supplementary Figures

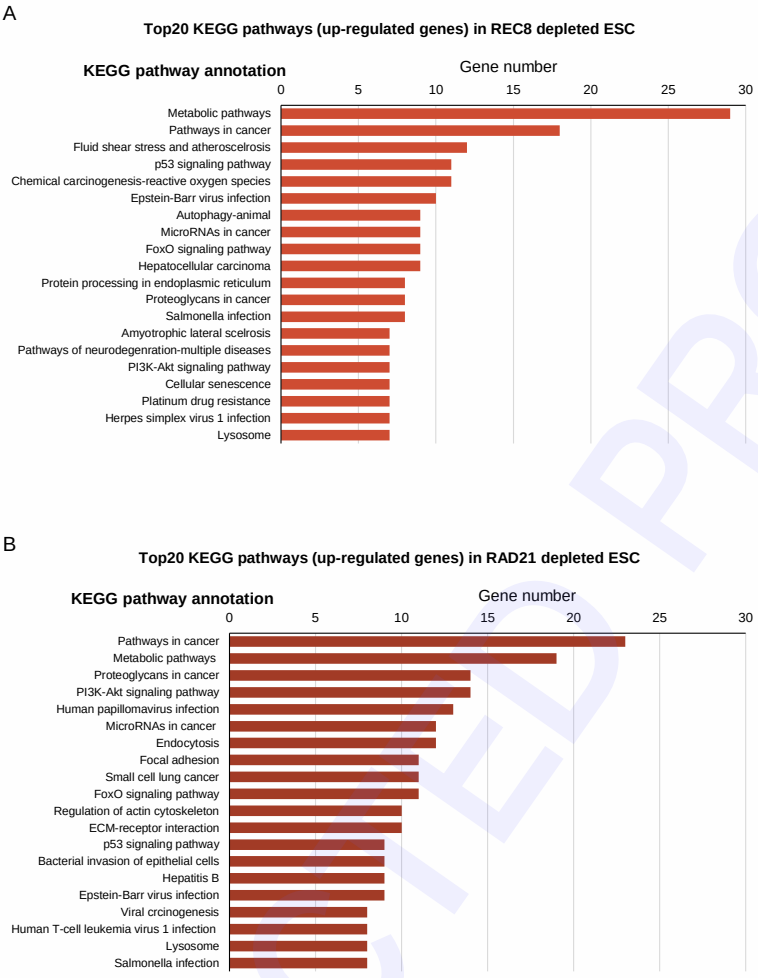

Supplementary Figure 1. TOP 20 KEGG pathways according to the number of upregulated genes in REC8- or RAD21-depleted ESC. KEGG (Kyoto Encyclopedia of Genes and Genomes) analysis was performed using the RNA sequencing data (Accession no. PRJNA725341). In REC8- or RAD21-depleted ESC, upregulated genes were sorted and classified according to the pathway involving the upregulated genes. (A) KEGG pathways involving the upregulated genes in REC8-depleted ESC. (B) KEGG pathways involving the upregulated genes in RAD21-depleted ESC.

A

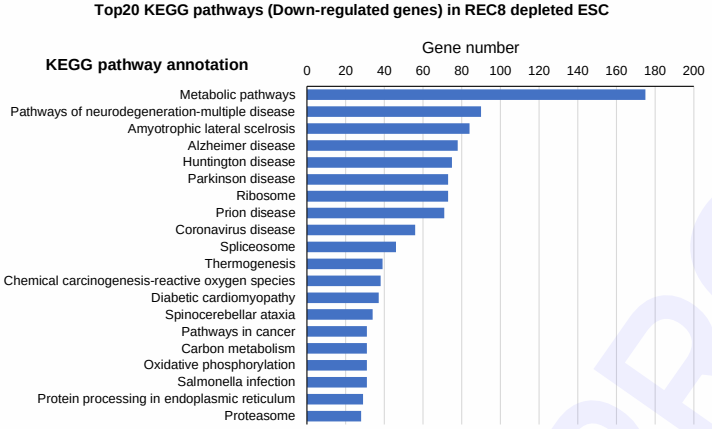

B

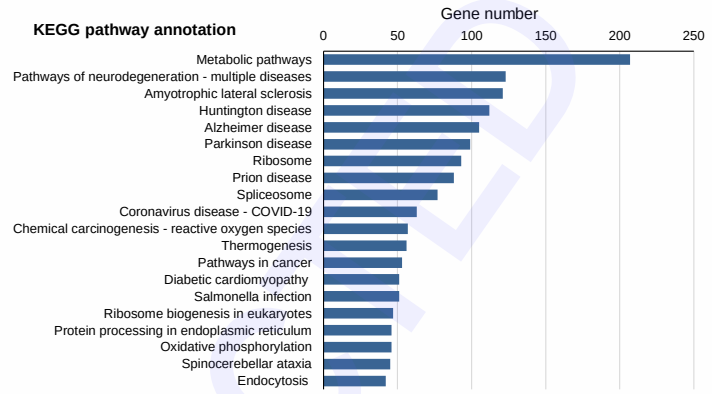

Supplementary Figure 2. TOP 20 KEGG pathways according to the number of downregulated genes in REC8- or RAD21-depleted ESC. KEGG (Kyoto Encyclopedia of Genes and Genomes) analysis was performed using the RNA sequencing data (Accession no. PRJNA725341). In REC8- or RAD21-depleted ESCs, downregulated genes were sorted and classified according to the pathway involving the upregulated genes. (A) KEGG pathways involving the downregulated genes in REC8-depleted ESCs. (B) KEGG pathways involving the downregulated genes in RAD21-depleted ESCs.

Supplementary Figure 3

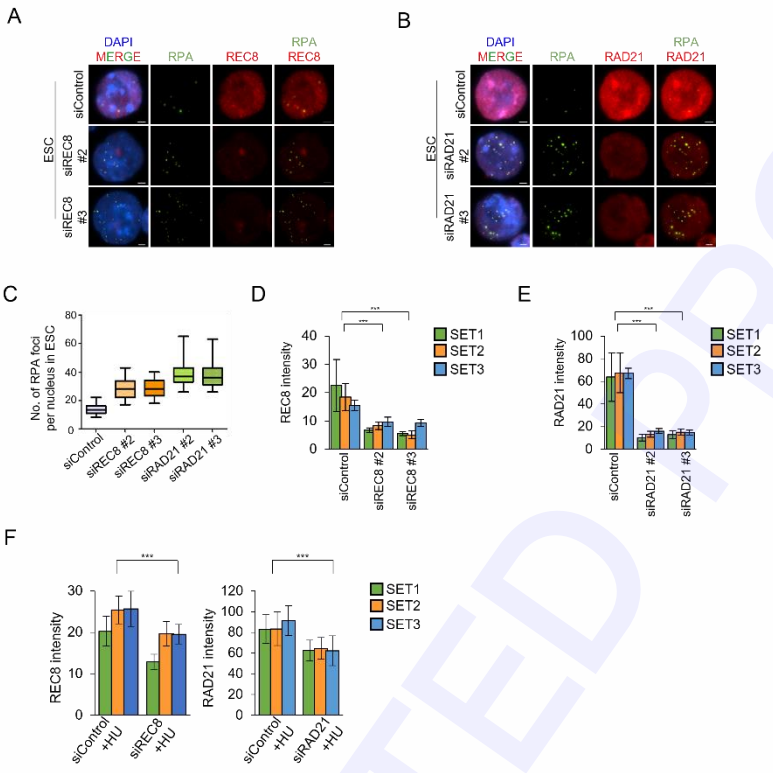

Supplementary Figure 3. RPA foci number and intensity of REC8 and RAD21 after siRNA treatment. (A, B) Representative images of REC8- or RAD21-depleted ESC. Another two siRNA sequences against REC8 or RAD21 were treated in ESC. RPA focus number per nucleus was counted (C) and intensity of kleisin factor was measured (D, E). Bars in whisker plots indicate minimum to maximum value. Error bars in bar graphs represent mean ± SD. Three independent experiments were carried out and 40 cells per experiment were measured. (F) REC8 and RAD21 intensities were measured under the following conditions: siControl and HU treatment and siRNA treatment against REC8 or RAD21 and HU. Three independent experiments were performed (sets 1, 2, and 3).

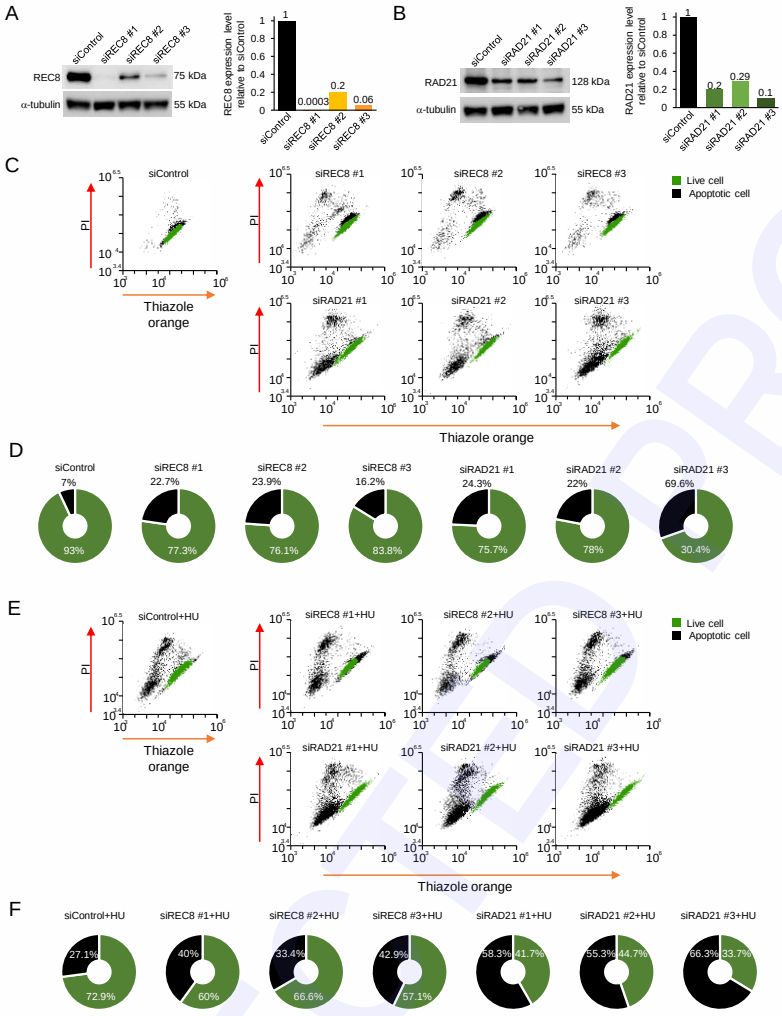

Supplementary Figure 4. siRNA against REC8 or RAD21 validation via cell viability assay. Three candidates of siRNA sequence targeting REC8 or RAD21 were selected, and cell viability assay was analyzed. In ESCs, REC8 or RAD21 was depleted using three siRNA candidates, and cell viability was measured (A). (B) Quantification of the cell viability of (A). The proportion of live cells was represented in green color, and the proportion of apoptotic cells was shown in black in doughnut graphs. (C) Cell survival rate under α-kleisin factor depletion and DNA damage condition in ESCs. Under DNA damage condition with HU, the proportion of live cell (green) or apoptotic/dead cell rate (black) in REC8- or RAD21-depleted ESCs was quantified (D-F).

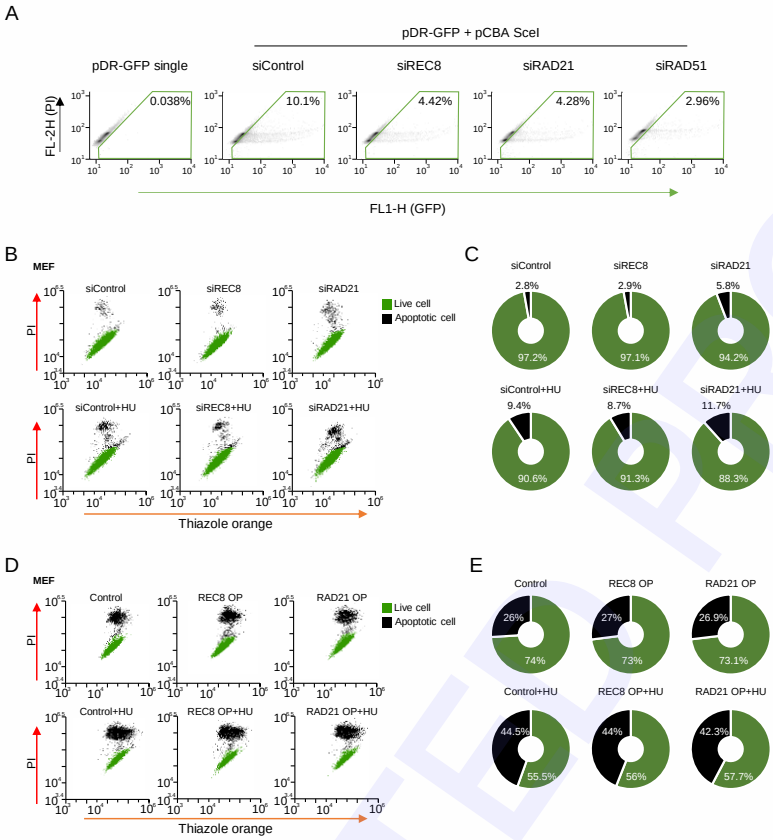

Supplementary Figure 5. Cell viability and homologous recombination efficiency after gene knockdown. (A) GFP expression in ESCs generated via pDR-GFP analysis. The pDR-GFP and pCBA-SceI plasmids were transfected into ESCs to confirm the efficiency of homologous recombination. The proportion of GFP-positive cells was determined via FACS analysis. (B-E) Cell survival rate was measured via FACS analysis under α-kleisin factor depletion condition or overexpression of REC8 or RAD21 condition with/without HU in MEF cells stained with thiazole orange and propidium iodide. siREC8- or siRAD21-treated MEF or siREC8- and HU treated- or siRAD21- and HU-treated MEF cell was analyzed using FACS (B). (D) Quantification of cell viability in α-kleisin factor-depleted MEF or α-kleisin factor-depleted and DNA-damaged MEF. Green represents the proportion of live cells, and black shows the proportion of apoptotic cells. The cell viability rate in REC8- or RAD21-overexpressed MEF or REC8- or RAD21-overexpressed with DNA-damaged MEF was measured. The proportion of live cell/apoptotic cells was quantified in (E). Green indicates the ratio of live cells, and black corresponds to the ratio of apoptotic cells.

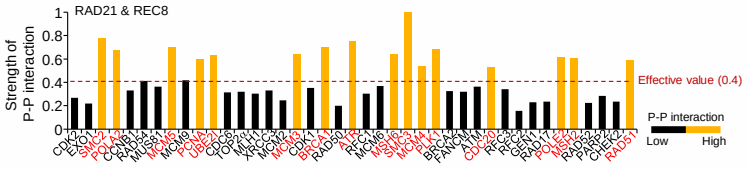

Supplementary Figure 6. Protein–protein interaction with REC8 and RAD21.

Data are visualized using Cytoscape software. The X-axis shows factors interacting with RAD21 and REC8. The Y-axis represents the strength of the interaction between α-kleisin protein and other factors. The yellow bar graph presents the strengths of protein–protein interactions that were above the effective value (0.4). The black bars indicate the interactions that were lower than the effective values.

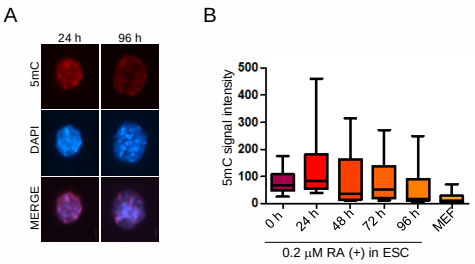

Supplementary Figure 7. DNA methylation levels during stem cell differentiation.

(A, B) DNA methylation pattern during cell differentiation induced by retinoic acid. 5mC staining intensity was analyzed by measuring the immunofluorescence intensity of anti-5mC antibody.

Supplementary Table 1. siRNA sequences

Sequence name	Sequence
REC8 #1	5′-GAGCAAAGAUGUUCUACUA-3′
REC8 #2	5′-ACUAUCCUAACGUGCUUCA-3′
REC8 #3	5′-GAGAUCAGUCGAGGAGACU-3′
RAD21 #1	5′-GAGCUAGUGAUAACUCACU-3′
RAD21 #2	5′-GAGUCUUAGGACCUCUGAU-3′
RAD21 #3	5′-GUGACUUCGGAAUGGAUGA-3′
RAD51	5′-GAAUUGAGACUGGAUCUAU-3′